Journal of Power Sources 183 (2008) 43–48

Contents lists available at ScienceDirect

Journal of Power Sources

journal homepage: www.elsevier.com/locate/jpowsour

Preparation and electrochemical properties of Sr-doped Nd_2NiO_4 cathode materials for intermediate-temperature solid oxide fuel cells

Li-Ping Sun[a], Qiang Li[a], Hui Zhao[a,*], Li-Hua Huo[a], Jean-Claude Grenier[b]

[a] Laboratory of Functional Materials, School of Chemistry and Materials Science, Heilongjiang University, Harbin 150080, PR China
[b] Bordeaux Institute of Condensed Matter Chemistry, Pessac 33608, France

ARTICLE INFO

Article history:
Received 24 August 2007
Received in revised form 30 April 2008
Accepted 2 May 2008
Available online 7 May 2008

Keywords:
Intermediate-temperature solid oxide fuel cell (IT-SOFC)
NSN cathode material
Electrode reaction

ABSTRACT

Cathode materials $Nd_{2-x}Sr_xNiO_4$ were prepared by the glycine-nitrate process and characterized by X-ray diffraction (XRD), scanning electron microscopy (SEM), AC impendence spectroscopy and DC polarization method, respectively. The results show that no reaction occurred between the electrode and the CGO electrolyte at 1100 °C and the electrode formed good contact with the electrolyte after being sintered at 1000 °C for 4 h. The rate-limiting step for oxygen reduction reaction on $Nd_{1.6}Sr_{0.4}NiO_4$ electrode changed with oxygen partial pressure and measurement temperature. The $Nd_{1.6}Sr_{0.4}NiO_4$ electrode gave a polarization resistance of 0.93 Ω cm^2 at 700 °C in air, which indicates that $Nd_{2-x}Sr_xNiO_4$ electrode is a promising cathode material for intermediate-temperature solid oxide fuel cell (IT-SOFC).

© 2008 Elsevier B.V. All rights reserved.

1. Introduction

High operating temperature of SOFC results in high cost and materials compatibility challenges. Reducing the operating temperature of SOFC is the most important issue to settle for its practical use [1,2]. It has been found that, at intermediate temperature, the performance of cathode tends to limit the cell's performance [3–7]. Considerable investigations have been done on various perovskite-type oxides to improve the cathode performance at intermediate temperature [8–10]. Among these oxides, the cobalt-based materials were given more recognition because of their high conductivity and good electrochemical property. However, the thermal expansion coefficients (TECs) of some cobaltite phases are 50–300% higher with respect to the possible electrolyte candidates, such as $La_{0.9}Sr_{0.1}Ga_{0.8}Mg_{0.2}O_{2.85}$ (LSGM) and $Ce_{0.9}Gd_{0.1}O_{2-\delta}$ (CGO) [11–13]. Due to thermomechanical incompatibility, long-term stability of the cells with cobalt-based cathode layers appears very problematic.

Another group of materials promising for intermediate-temperature solid oxide fuel cell (IT-SOFC) cathodes refers to the A_2BO_4 oxides with the perovskite-related K_2NiF_4-type structure. It is found that most of these compounds exhibit relatively high oxygen ionic diffusivity, compatible TECs with solid electrolytes, and predominantly P-type electronic conductivity in whole $p(O_2)$ range where the K_2NiF_4-type phases exist.

At present, most of the researches are concentrated on the mixed conducting materials related to rare earth nickel oxides, $Ln_2NiO_{4+\delta}$ (Ln = La, Pr or Nd). The origin of oxygen overstoichiometry and oxygen diffusion in these materials has been extensively discussed [14–18]. It has been shown that substitutions on the B site of A_2BO_4 compounds affect simultaneously the amount of oxygen stoichiometry and the transport properties [19,20]. As a consequence, $La_2Ni_xCo_{1-x}O_4$ and $La_2Ni_{1-x}Cu_xO_4$ have been widely studied [21,22]. From the reported oxygen-diffusion results it appears that these doped materials show improved oxygen-diffusion coefficients, which often has a positive effect on the cathode performance. Besides the doping strategy on the B site, partial substitution on the A site of the A_2BO_4 compounds can increase the oxygen vacancy, enhance the electric conductivity and oxygen-diffusion coefficient.

Nie et al. reported that the Sr-doped $A_{2-\alpha}A'_\alpha BO_4$ (A = Pr, Sm; A′ = Sr; B = Mn, Ni) has better cathodic properties than the undoped materials [23]. In our previous study, a similar result was found in Sr-doping in La_2NiO_4 and Sm_2NiO_4 materials [24,25].

$Nd_2NiO_{4+\delta}$ has been reported to exhibit promising electrocatalytic activity to oxygen reduction reaction when used as cathode for IT-SOFC [26,27]. The oxygen-diffusion coefficient of $Nd_2NiO_{4+\delta}$ is also much higher than that of $La_2NiO_{4+\delta}$ [16,26]. In continuing our studies of nickelate-based mixed conducting materials for SOFC cathode applications, the electrochemical properties of Sr-doped Nd_2NiO_4 materials supported on $Ce_{0.9}Gd_{0.1}O_{1.95}$ (CGO) electrolyte

* Corresponding author. Tel.: +86 45186608040; fax: +86 45186608040.
E-mail address: zhaohui98@yahoo.com (H. Zhao).

0378-7753/$ – see front matter © 2008 Elsevier B.V. All rights reserved.
doi:10.1016/j.jpowsour.2008.05.001

and the kinetics of oxygen reduction on these electrodes are studied.

2. Experimental

$Nd_{2-x}Sr_xNiO_4$ (x = 0.2, 0.4, 0.6 and 0.8) powders were synthesized using the glycine–nitrate process (GNP). According to the formula, stoichiometric amount of $Nd(NO_3)_3$, $Sr(NO_3)_2$ and $Ni(NO_3)_2$ were mixed in a beaker to form a solution, and then glycine (aminoacetic acid, $H_2NCH_2CO_2H$) was added into the nitrate solution at 1:2 molar ratio of metal ions/glycine according to propellant chemistry. After drying and firing, the resultant powders were calcined in air at 1100 °C for 12 h. The obtained materials were abbreviated as NSN1802 for $Nd_{1.8}Sr_{0.2}NiO_4$, NSN1604 for $Nd_{1.6}Sr_{0.4}NiO_4$, and so on. $Ce_{0.9}Gd_{0.1}O_{1.9}$ (CGO) powders were prepared according to Ref. [28]. The CGO powders were pressed uniaxially at 220 MPa and then sintered at 1400 °C for 10 h to form a densified pellet. The $Nd_{2-x}Sr_xNiO_4$ powders were mixed with terpineol to form a slurry, and subsequently painted on one side of the CGO electrolyte to form an electrode area of 0.5 cm^2, used as working electrode (WE). Platinum paste was painted on the other side of the CGO pellet in symmetric configuration, as the counter electrode (CE). A Pt wire was used as reference electrode (RE) and put on the same side of the working electrode. The cathodes were first heated at 400 °C for 2 h to eliminate organic binders, followed by sintering at different temperatures for 4 h in air, with a heating/cooling rate of 3 °C min^{-1}. The sample was characterized using X-ray diffraction instrument (Rigaku, D/MAX-3B) and scanning electron microscopy (SEM) (Hitachi, S-4700 FEG), respectively. The phase transition of the samples was investigated with a Setsys Evolution TG–DTA system (SETARAM, France) from room temperature to 900 °C. Thermal expansion behavior was measured with Setsys Evolution TMA system. The measurements were carried out in air with a heating rate of 5 °C min^{-1} from room temperature to 1000 °C. The impedance spectra were recorded over the frequency range 1 MHz to 0.1 Hz using Autolab PGStat30. The measurements were performed at OCV as a function of temperature (500–700 °C) and oxygen partial pressure (in an N_2/O_2 mixed atmosphere). The DC polarization experiments were performed by the chronoampermetry methods, as that explained in Ref. [29].

3. Results and discussions

Phase purity and chemical compatibility of $Nd_{2-x}Sr_xNiO_4$ with CGO electrolyte were first investigated. Fig. 1 shows the X-ray diffraction (XRD) patterns of the obtained NSN powders and NSN1604–CGO mixtures calcined at 1100 °C for 4 h. It can be seen that NSN powders made by the glycine–nitrate process crystallize in body-centered tetragonal symmetry, consisting with K_2NiF_4 structure. No impurity was found when the strontium doping concentration was up to x = 0.8. NSN1604 and CGO retained their own structures unchanged in the NSN1604–CGO mixtures after being sintered at 1100 °C for 4 h, indicating that no chemical reaction occurs between the two components. This result revealed that NSN1604 had good chemical compatibility with the CGO electrolyte. In order to investigate the structural stability of the samples, TG–DTA test was carried out under air. The results showed that there is no phase transition occurred from room temperature to 900 °C for these samples. So it can be concluded that the $Nd_{2-x}Sr_xNiO_4$ materials are structurally stable under our experimental conditions.

The expansion behaviors of specimens are shown in Fig. 2. It was observed that the thermal expansion coefficients increased with the Sr doping concentration. This is due to the loss of lattice oxygen

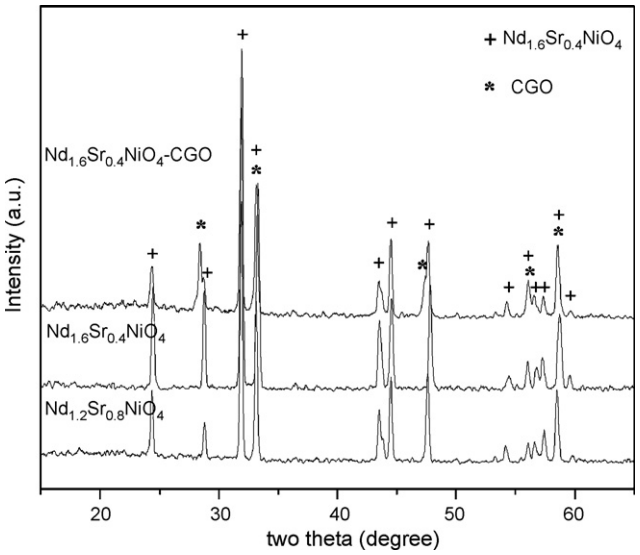

Fig. 1. XRD patterns of NSN and NSN1604–CGO mixtures after heated at 1100 °C for 4 h in air.

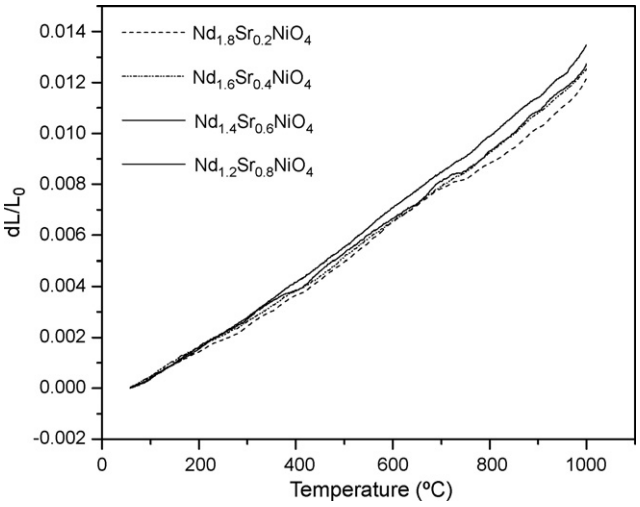

Fig. 2. Line thermal expansion curves in air for $Nd_{2-x}Sr_xNiO_4$ (x = 0.2, 0.4, 0.6 and 0.8).

and the formation of oxygen vacancy, a process that is enhanced as the Sr-doping content increases [30]. The average values of TEC (50–1000 °C) are listed in Table 1. Clearly the TECs of $Nd_{2-x}Sr_xNiO_4$ are close to that of CGO.

Fig. 3a and b shows the typical Nyquist and Bode plot for NSN cathode sintered at different temperatures, respectively. In the Bode plots, peaks in the imaginary part correspond to the summit frequencies of physicochemical process that occurred on the cathode. From Fig. 3a and b, one major process can be identified within the measurement frequency domain. Although with careful inspection, it seems that another small arc exists at high-frequency

Table 1
Thermal expansion in air of $Nd_{2-x}Sr_xNiO_4$ (x = 0.2, 0.4, 0.6 and 0.8)

Composition	TEC ($\times 10^{-6}$ K^{-1}) (50–900 °C)
$Nd_{1.8}Sr_{0.2}NiO_4$	12.8
$Nd_{1.6}Sr_{0.4}NiO_4$	13.0
$Nd_{1.4}Sr_{0.6}NiO_4$	13.1
$Nd_{1.2}Sr_{0.8}NiO_4$	14.4

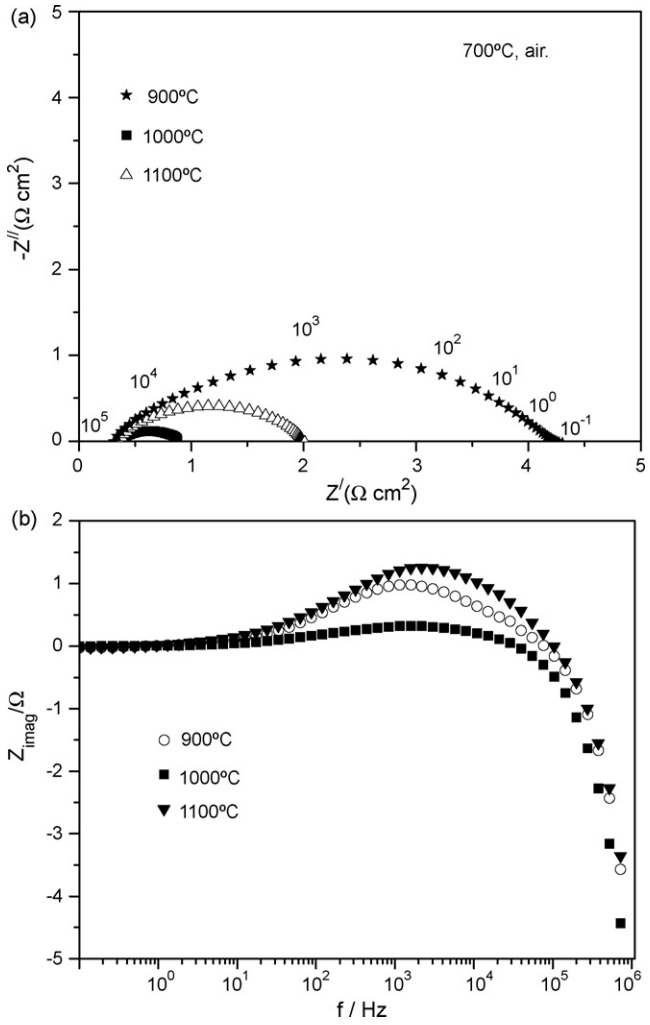

Fig. 3. Nyquist plots (a) and Bode plots (b) of the $Nd_{1.6}Sr_{0.4}NiO_4$ cathode sintered at different temperature for 4 h and then measured at 700 °C in air.

side. It is however hard to separate them, due to the serious overlap of the two arcs. We should note that in a previous paper about oxygen electrode reaction on $Ln_2NiO_{4+\delta}$ (Ln = La, Nd and Pr) materials, three conjunctive arcs were observed from high-frequency to low-frequency range [27]. The obvious difference maybe comes from the different preparation methods of cathode materials and the selections of different electrolyte materials. The intercept value of the impedance arcs with the real axis at high-frequency side corresponds to the resistance of the electrolyte and lead wires, while the value between the high-frequency x-axis intercept and the low-frequency one is attributed to the total polarization resistance (R_p) of $Nd_{1.6}Sr_{0.4}NiO_4$ electrode.

In the experiments, we found that the sintering conditions had remarkable effects on the electrode performance. From the impedance spectrum, we observed that the electrode polarization was relatively large when the sintering temperature was low (900 °C). When the sintering temperature was 1000 °C, R_p reduced to the lowest value and then it increased again when the sintering temperature was up to 1100 °C. The effects of sintering temperature on R_p can be understood from the microstructure evolution of $Nd_{1.6}Sr_{0.4}NiO_4$ electrode. The SEM results of the $Nd_{1.6}Sr_{0.4}NiO_4$ electrode on CGO electrolyte after sintering at different temperatures for 4 h are given in Fig. 4. It was observed that NSN particles formed poor contact with each other when the sintering temperature was 900 °C (Fig. 4a). After being sintered at 1000 °C, a fine microstructure with moderate porosity and well-necked particles has been formed, and the interface combined well between NSN electrode and CGO electrolyte. The average particle size was about 1.5 μm, and the thickness of the electrode was about 25 μm (Fig. 4b and d). This kind of microstructure is benefit for the improved cathode property, as that observed in Fig. 2. When the electrode was sintered at 1100 °C for 4h, however, particle agglomeration phenomenon was observed (Fig. 4c). This effect decreased the electrode porosity and triple phase boundary (TPB) length, resulting in the increase of R_p. The similar over-sintering effect has been observed before in the other cathode materials [24].

Fig. 5 shows the behavior of polarization resistance as a function of temperature for the $Nd_{2-x}Sr_xNiO_4$ cathodes. A linear relationship between the $\log(R_p)$ and $1000\,T^{-1}$ was obtained. The activation energy (determined by the slope of the interpolated straight lines) is around 1.0 eV for NSN electrodes. It was found that the polarization resistance decrease first with the increase of Sr doping concentration, and $Nd_{1.6}Sr_{0.4}NiO_4$ gave the lowest polarization resistance (~0.93 ohm cm^2) at 700 °C in air. After that, the polarization resistance increases again. This value (~0.93 ohm cm^2) is lower than the reported Nd_2NiO_4 electrode material [26]. Hereafter, all of the electrode behavior studies are performed on $Nd_{1.6}Sr_{0.4}NiO_4$ material.

At present, this anomalous behavior of polarization resistance to the Sr doping concentration is difficult to understand. We propose

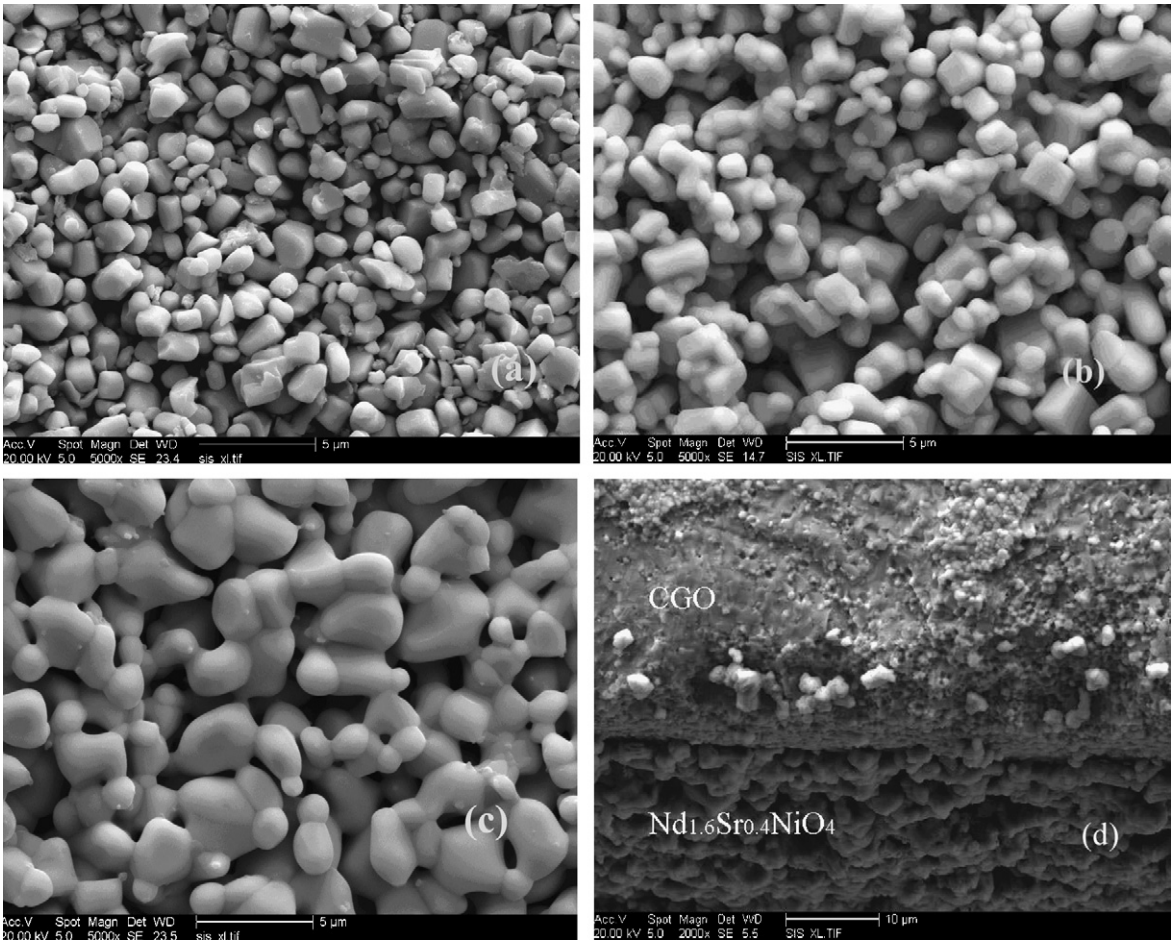

Fig. 4. SEM images of the $Nd_{1.6}Sr_{0.4}NiO_4$ electrode sintered at 900 °C (a); 1000 °C (b); 1100 °C (c); the cross-section image of the test cell (d).

that this phenomena is related to the complex oxygen evolution behavior that occurred in Sr doping Nd_2NiO_4 material [31]. As we know, Nd_2NiO_4 has the ability to accommodate excess oxygen in the structure, which promotes the oxygen ions transport, and therefore the cathodic performance of the material. With moderate Sr doping, however, the excess oxygen disappears, and chemical stoichiometric compound will form [31]. Further doping will lead to the formation of oxygen vacancy in the lattice, which again improves the cathodic performance. Finally high concentration of doping will generate the complex defects of oxygen vacancy, and retard the oxygen ion transport in the material.

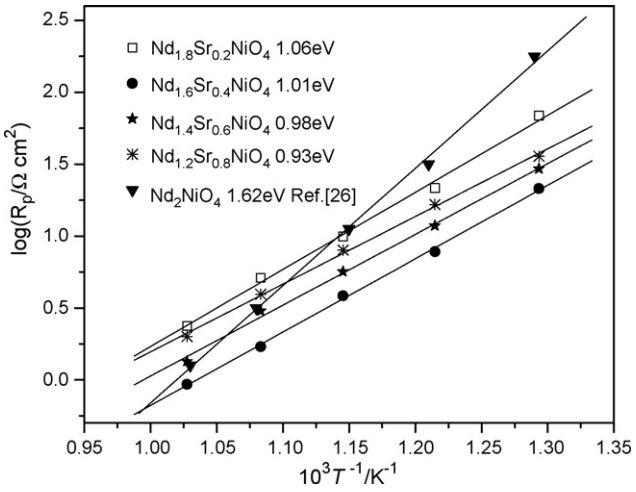

Fig. 5. Temperature dependence of the polarization resistances (R_p) for $Nd_{2-x}Sr_xNiO_4$ electrodes measured over a temperature range of 500–700 °C in air.

In order to clarify the effect of oxygen partial pressure on the cathode processes, a comparative study of Nyquist and Bode plots at different oxygen partial pressure were carried out. As shown in Fig. 6a and b, clearly only one major process can be identified, and this process changes systematically with the measuring temperature and oxygen partial pressure. The R_p was used to study the effect of oxygen partial pressure on the electrode performance as a function of temperature. Generally, R_p varies with the oxygen partial pressure according to the following equation:

$$R_p = R_p^0 (P_{O_2})^n$$

$$n = 1, \quad O_2(g) \Leftrightarrow O_{2,ads.}$$

$$n = \frac{1}{2}, \quad O_{2,ads.} \Leftrightarrow 2O_{ads.}$$

$$n = \frac{1}{4}, \quad O_{ads.} + 2e^{/} + V_O^{\bullet\bullet} \Leftrightarrow O_O^x$$

$$n = \frac{1}{10}, \quad O_{TPB}^{2-} + V_O^{\bullet\bullet} \Leftrightarrow O_O^x$$

The value of n could give useful information about the type of species involved in the reactions [32,33].

The dependence of polarization resistance on oxygen partial pressure was shown in Fig. 7. The $P_{O_2}^{1/4}$ relationship was considered

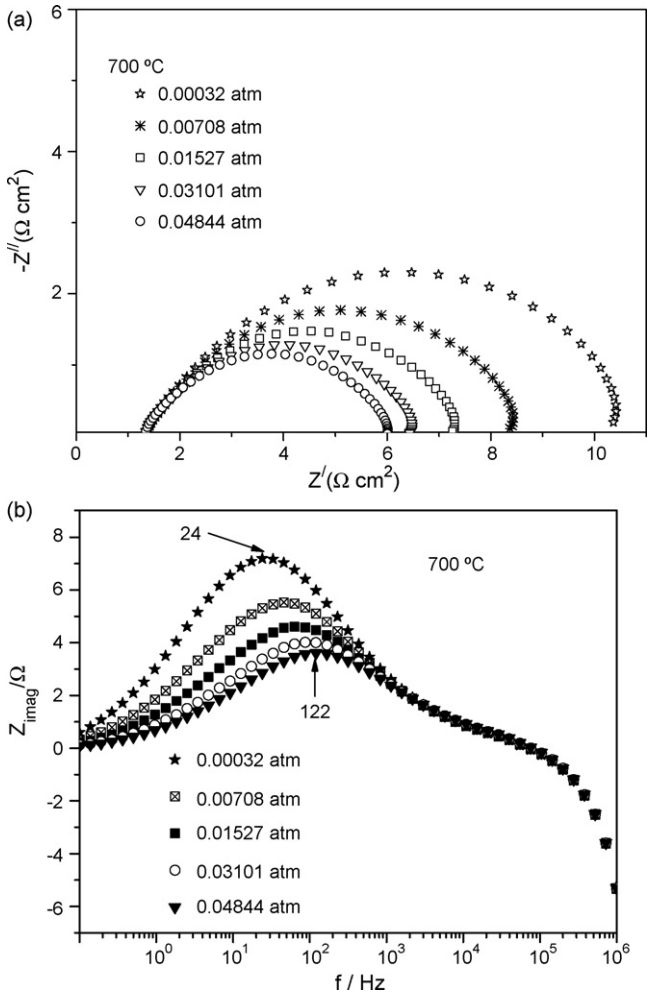

Fig. 6. Impedance spectra for the $Nd_{1.6}Sr_{0.4}NiO_4$ cathode on CGO at 700 °C under various oxygen partial pressures (a: Nyquist plot; b: Bode plot).

as the contribution of the charge transfer process on the electrode, which was observed before for Nd_2NiO_4 cathode [26]. In a previous study, the $P_{O_2}^{1/10}$ relationship has been observed for LSM-YSZ cathode. It was due to the oxygen ion transfer from the TPB to the electrolyte [33]. Our results indicated that at low oxygen partial pressure (less than 0.01 atm), n value is 0.1, and above 0.01 atm, n value is in the range of 0.21–0.25. The n values in the two regions remain almost unchanged between 600 °C and 700 °C. Therefore, we conclude that two different kinds of reaction rate-limiting step exist on the $Nd_{1.6}Sr_{0.4}NiO_4$ cathode, depending on the oxygen partial pressure. At low oxygen partial pressure (less than 0.01 atm), oxygen ion transfer from the $Nd_{1.6}Sr_{0.4}NiO_4$ electrode to CGO electrolyte is the rate-limiting step. Whereas at high oxygen partial pressure, the charge transfer reaction becomes more important. The complex cathode behavior observed for $Nd_{1.6}Sr_{0.4}NiO_4$ material is partially due to the easy variation of oxygen stoichiometry of this compound. The similar behavior has been observed in our previous research of $La_{2-x}Sr_xCuO_{4-\delta}$ materials [34].

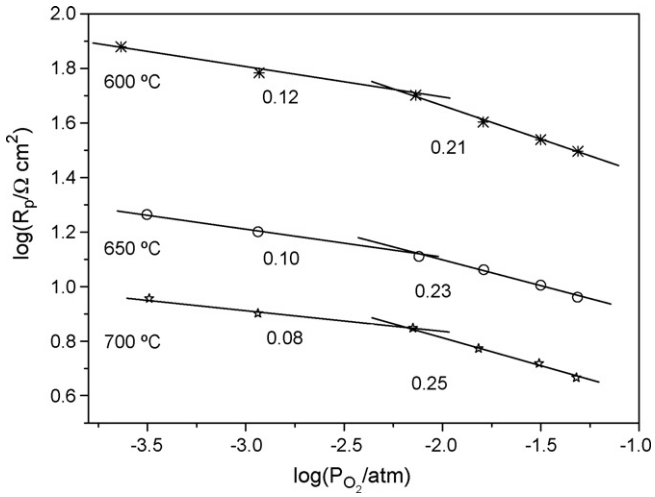

Fig. 7. Dependence of R_p on oxygen partial pressure for $Nd_{1.6}Sr_{0.4}NiO_4$ cathode at different temperatures.

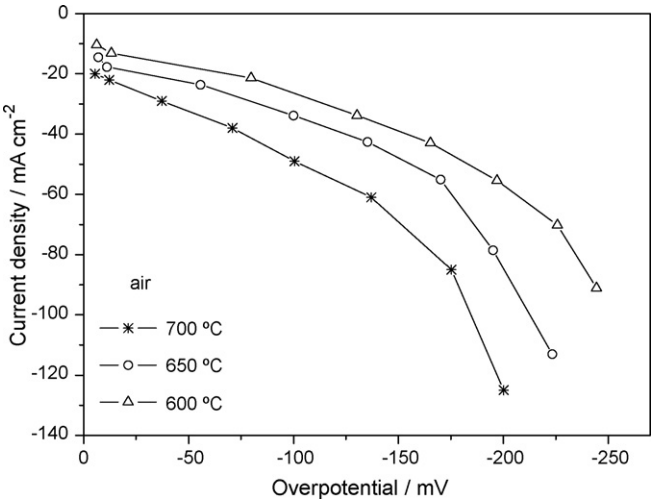

Fig. 8. The overpotential–current density curves for $Nd_{1.6}Sr_{0.4}NiO_4$ cathode measured in air at various temperatures (after IR compensation).

Cathodic overpotential is an important parameter for SOFC. The cathodic overpotential as a function of current density at different temperatures was plotted in Fig. 8. It was observed that under the same current density the cathodic overpotential decreases with the increase of measurement temperature. When the current density reached 125 mA cm^{-2} at 700 °C in air, the cathodic overpotential was 200 mV, which is lower than the reported Nd_2NiO_4 cathode materials in literature [26]. As we expected, doping of strontium in the lattice results in the generation of oxygen vacancies, which promote the mobility of the oxygen ions in the lattice. Therefore, the amount of absorbed oxygen on the electrode surface and the migration of oxygen to the TPB or diffusion to the electrode/electrolyte interface can be strongly enhanced.

4. Conclusions

(1) $Nd_{2-x}Sr_xNiO_4$ cathode forms good contact with CGO electrolyte after sintering at 1000 °C for 4 h and no reaction was found between $Nd_{1.6}Sr_{0.4}NiO_4$ electrode and CGO electrolyte.
(2) The rate-limiting step for oxygen reduction on the electrode changed with oxygen partial pressure and temperature.
(3) $Nd_{1.6}Sr_{0.4}NiO_4$ exhibited the highest cathode performance. The lowest area specific resistance obtained at 700 °C in air is 0.93 Ω cm^2, and the highest current density is 125 mA cm^{-2} at an overpotential of 200 mV.

Acknowledgements

The Project was supported by Science Foundation for Distinguished Young Scholars of Heilongjiang Province and Key Project of Chinese Ministry of Education (206044 and 205050).

References

[1] H. Fukunaga, M. Koyama, N. Takahashi, C. Wen, K. Yamada, Solid State Ionics 132 (2000) 279–285.
[2] H. Fukunaga, M. Ihara, K. Sakaki, K. Yamada, Solid State Ionics 86 (1996) 1179–1185.
[3] E. Maguire, B. Gharbage, F.M.B. Margues, J.A. Labrincha, Solid State Ionics 127 (2000) 329–335.
[4] A. Endo, H. Fukunaga, C. Wen, K. Yamada, Solid State Ionics 135 (2000) 353–358.
[5] Y.K. Lee, J.Y. Kim, Y.K. Lee, J. Power Sources 115 (2003) 219–228.
[6] T. Ioroi, T. Hara, Y. Uchimoto, Z. Ogumi, Z. Takehara, J. Electrochem. Soc. 144 (1997) 1362–1370.
[7] N.Q. Minh, J. Am. Ceram. Soc. 76 (1993) 563–588.
[8] C.R. Xia, R. William, F.L. Chen, M.L. Liu, Solid State Ionics 149 (2002) 11–19.
[9] K. Huang, M. Feng, J.B. Goodenough, C. Milliken, J. Electrochem. Soc. 144 (1997) 3620–3624.
[10] R. Maric, S. Ohara, T. Fukui, H. Yoshida, M. Nishimura, T. Inagaki, K. Miura, J. Electrochem. Soc. 146 (1999) 2006–2010.
[11] K. Huang, M. Feng, J.B. Goodenough, M. Schmerling, J. Electrochem. Soc. 143 (1996) 3630–3636.
[12] H. Hayashi, M. Suzuki, H. Inaba, Solid State Ionics 128 (2000) 131–139.
[13] V.V. Kharton, F.M. Figueiredo, L. Navarro, E.N. Naumovich, A.V. Kovalevsky, A.A. Yaremchenko, A.P. Viskup, A. Carneiro, F.M.B. Marques, J.R. Frade, J. Mater. Sci. 36 (2001) 1105–1117.
[14] C. Allançon, P. Odier, J.M. Bassat, J.P. Loup, J. Solid State Chem. 131 (1997) 167–172.
[15] S.J. Skinner, J.A. Kilner, Ionics 5 (1999) 171–174.
[16] S.J. Skinner, J.A. Kilner, Solid State Ionics 135 (2000) 709–712.
[17] L. Minervini, R. Grimes, J. Kilner, K. Sickafus, J. Mater. Chem. 10 (2000) 2349–2354.
[18] V. Kharton, A. Viskup, A. Kovalesvsky, E. Naumovich, F. Marques, Solid State Ionics 143 (2001) 337–353.
[19] V.V. Kharton, A. Viskup, E. Naumovich, F. Marques, J. Mater. Chem. 9 (1999) 2623–2629.
[20] V. Vashook, I. Yushkevich, L.V. Kokhanovsky, L.V. Makhnach, S. Tolochko, I.F. Kononyuk, H. Ullmann, H. Altenburg, Solid State Ionics 119 (1999) 23–30.
[21] J.A. Kilner, C.K.M. Shaw, Solid State Ionics 154 (1999) 523–527.
[22] E. Boehm, J.M. Bassat, M.C. Steil, P. Dordor, F. Mauvy, J.C. Grenier, Solid State Sci. 5 (2003) 973–981.
[23] H.W. Nie, T.L. Wen, S.R. Wang, Y.S. Wang, U. Guth, V. Vashook, Solid State Ionics 177 (2006) 1929–1932.
[24] Q. Li, Y. Fan, H. Zhao, L.P. Sun, L.H. Huo, J. Power Sources 167 (2007) 64–68.
[25] Q. Li, Y. Fan, H. Zhao, L.H. Huo, Chin. J. Inorg. Chem. 11 (22) (2006) 2025–2030.
[26] F. Mauvy, J.M. Bassat, E. Boehm, J.P. Manaud, P. Dordor, J.C. Grenier, Solid State Ionics 158 (2003) 17–28.
[27] F. Mauvy, C. Lalanne, J.M. Bassat, J.C. Grenier, H. Zhao, P. Dordor, P. Stevens, J. Eur. Ceram. Soc. 25 (2005) 2669–2672.
[28] S. Zha, A. Moore, H. Abernathy, M. Liu, J. Electrochem. Soc. 151 (8) (2004) A1128–A1133.
[29] H. Zhao, L.H. Huo, L.P. Sun, L.J. Yu, S. Gao, J.G. Zhao, Mater. Chem. Phys. 88 (2004) 160–166.
[30] Y.S. Wang, H.W. Nie, S.R. Wang, T.L. Wen, U. Guth, V. Valshook, Mater. Lett. 60 (2006) 1174–1178.
[31] J. Alonso, M. Vallet-Regf, J.M. González-Calbet, Solid State Ionics 66 (1993) 219–223.
[32] E. Sicbeit, A. Hammouche, M. Kleitz, Electrochim. Acta 40 (1995) 1741–1753.
[33] J.D. Kim, G.D. Kim, J.W. Moon, Y. Park, W.H. Lee, K. Kobayashi, M. Nagai, C.E. Kim, Solid State Ionics 143 (2001) 379–389.
[34] Q. Li, H. Zhao, L.H. Huo, L.P. Sun, X.L. Cheng, J.C. Grenier, Electrochem. Commun. 9 (2007) 1508–1512.